Submitted to Astrophys.J.

SLAC-PUB-12670
astro-ph/0707.0737
July 2007

Draft to ApJ
Preprint typeset using LaTeX style emulateapj v. 11/26/04

THE CAUSES OF HALO SHAPE CHANGES INDUCED BY COOLING BARYONS: DISKS VERSUS SUBSTRUCTURES

Victor P. Debattista[1,2], Ben Moore[3], Thomas Quinn[1], Stelios Kazantzidis[4], Ryan Maas[1], Lucio Mayer[3], Justin Read[3], Joachim Stadel[3]

(Dated: *Draft version on July 6, 2007*)
Draft to ApJ

ABSTRACT

Cold dark matter cosmogony predicts that dark matter halos should be triaxial, whereas observations suggest that halos are rounder. The difference between theory and observation is mostly likely explained by the effect of baryons since their condensation within triaxial dark matter halos is known to lead to rounder halos. This is usually thought to be due to the scattering of box orbits. In order to understand the process by which halos become rounder, we present controlled simulations of disks grown adiabatically inside triaxial dark matter halos. After the disks are grown to full mass we adiabatically evaporate the disks and compare the initial and final shapes of the halos. We find that while the halos are substantially rounder while the disk is at full mass, their final shape after the disk is evaporated is not substantially different from the initial. Thus the condensation of baryons onto the center does not destroy enough of the box/box-like orbits to explain the full intermediate shape change. By following orbits of particles directly, we show that the character of individual orbits is not generally changed by the growing mass unless the disk is very centrally concentrated. Rather than being destroyed, we find that box orbits merely become rounder along with the global potential and that this is sufficient to explain most of the shape change. If chaos is enhanced by the growing baryonic mass then this must still have diffusion timescales of order a Hubble time or longer. We also explored the shape evolution in simulations in which we grew the masses of a small number of satellites, rather than of a central disk. In these experiments, the halo shape changes were substantially less reversible. We point out that since halo triaxiality can profoundly influence the evolution of disk galaxies, it is crucial that simulations of galaxy formation are able to reproduce the level and structure of satellites.

Subject headings: galaxies: evolution — galaxies: formation — galaxies: halos — dark matter

1. INTRODUCTION

The dark matter halos which form via hierarchal growth in the cold dark matter (CDM) cosmologies are generally triaxial with mean axial ratios $b/a \sim 0.6$ and $c/a \sim 0.4$, where $c < b < a$ are the short, intermediate and long axes, respectively (Bardeen et al. 1986; Barnes & Efstathiou 1987; Frenk et al. 1988; Dubinski & Carlberg 1991; Jing & Suto 2002; Bailin & Steinmetz 2005; Allgood et al. 2006). Observational constraints on halo shapes can be obtained from the Milky Way (Ibata et al. 2001; Johnston et al. 2005; Helmi 2004; Fellhauer et al. 2006), from polar ring galaxies (Schweizer et al. 1983; Sackett & Sparke 1990; Iodice et al. 2003), from X-ray isophotal shapes (Buote & Canizares 1994; Buote et al. 2002) and from gravitational lensing (Kochanek 1995; Bartelmann et al. 1995; Koopmans et al. 1998; Oguri et al. 2003). For disk galaxies, the ellipticity of the potential in the mid-plane, ϵ_Φ, also can be constrained through photometry and/or kinematics of stars or gas (e.g. Franx & de Zeeuw 1992; Huizinga & van Albada 1992; Kuijken & Tremaine 1994; Franx et al. 1994; Schoenmakers et al. 1997; Andersen et al. 2001; Debattista 2003; Barnes & Sellwood 2003). The general consensus from these studies is that dark matter halos are rounder than predicted by collisionless CDM simulations. But this need not be in disagreement with CDM since the condensation of baryons to the centers of halos has been shown to lead to rounder halos (Dubinski 1994; Kazantzidis et al. 2004). For example Kazantzidis et al. (2004) find that the principal axis ratios increase by $\sim 0.2 - 0.4$ in the inner regions (although triaxiality is not completely erased) extending to almost the virial radius.

Slowly rotating triaxial structures can be supported by centrophilic box orbits (Schwarzschild 1979; Gerhard & Binney 1985; Statler 1987; Udry & Martinet 1994; Fridman & Merritt 1997; Valluri & Merritt 1998). While early work suggested that cuspy triaxial systems could not be built of regular orbits (Merritt & Fridman 1996), more recent work (Poon & Merritt 2002) has shown that long-lived triaxial nuclei can be constructed from such orbits. Several studies have shown that, when a black hole is present, scattering of box orbits is responsible for causing an elliptical galaxy to become rounder, or at least axisymmetric (Lake & Norman 1983; Gerhard & Binney 1985; Norman et al. 1985; Merritt & Quinlan 1998; Valluri & Merritt 1998; Holley-Bockelmann et al. 2002; Kalapotharakos et al. 2004). These scattering events lead to a large number of orbits becoming chaotic. Chaos

[1] Astronomy Department, University of Washington, Box 351580, Seattle, WA 98195, USA debattis;trq;maasr@astro.washington.edu
[2] Brooks Prize Fellow
[3] Department of Theoretical Physics, University of Zürich, Winterthurerstrasse 190, CH-8057, Zürich, Switzerland moore;lucio;justin;stadel@physik.unizh.ch
[4] Kavli Institute for Particle Astrophysics and Cosmology, Department of Physics, Stanford University, P.O. Box 20450, MS 29, Stanford, CA 94309 USA; stelios@slac.stanford.edu.

Work supported in part by US Department of Energy contract DE-AC02-76SF00515

by itself, however, need not be a fundamental limit to forming long-lived triaxial structures: using orbit superposition, Poon & Merritt (2002) were able to build long-lived triaxial models of nuclei even in the presence of a large fraction ($\gtrsim 50\%$) of chaotic orbits. If axisymmetrization does occur, Gerhard & Binney (1985) predict that it may largely be confined to the center and occur gradually. The N-body simulations of a cored system by Merritt & Quinlan (1998) instead found that the axisymmetrization extends to the entire system and occurs on a crossing time for black holes of mass $\sim 2\%$ of the galaxy's mass. When instead the system is cuspy, Holley-Bockelmann et al. (2002) found that black holes do not lead to a global axisymmetrization of the system. Triaxial structures in disks, *i.e.* bars, can also be destroyed by central mass concentrations (CMCs). The main mechanism is again scattering by the central mass. Although bars are primarily supported by centrophobic loop (x_1) orbits, particles librating about the bar-supporting x_1 orbit family can get close to the center and then be scattered by a CMC. Simulations have shown that the required mass for a soft CMC (*i.e.* one with a scale of a few 100 parsec) is an unrealistically large $\sim 20\%$ of the disk mass, while the mass required of a hard CMC (few parsec scale) is $\sim 5\%$ of the disk mass (Shen & Sellwood 2004; Debattista et al. 2006), which is much larger than typical supermassive black holes.

It has often been assumed that the loss of triaxiality when baryons cool inside halos is partly or mostly due to the destruction of box orbits, which pass arbitrarily close to the center after a sufficiently long time. This is inspired by the similarity of this problem to that of a black hole growing inside a triaxial elliptical galaxy. Here we test whether box orbit scattering is responsible for triaxial halos becoming rounder when baryons cool inside them. We do this via simulations in which we slowly grow then evaporate disks inside triaxial halos. After the disks are grown we find that the halos become substantially rounder. But comparing their initial and final shapes when the disk mass is zero in both cases, we find that the changes are largely reversible. The destruction of box orbits being irreversible, halos should not recover their shapes if this is the main cause of the shape change. We also examine the effect of baryons condensing onto satellite substructure and find that irreversible changes in this case are substantially larger.

This paper is organized as follows: In Section 2 we discuss the N-body methods used in this paper. Section 3 presents the simulations. Section 4 presents a small number of randomly chosen box-like orbits taken from the particle distribution to show that most of these remain box-like through the entire evolution except when the baryons are very centrally concentrated. Our conclusions are presented in Section 5.

2. NUMERICAL METHODS

We formed prolate/triaxial halos via the merger of two or more spherical halos, as described in Moore et al. (2004). The initial spherical halos were generated from a distribution function using the method described in Kazantzidis et al. (2004) with the added refinement that each halo is composed of two mass species arranged on shells. The outer shell has more massive particles than the inner one, in order to increase the effective resolution in the central parts. In all mergers we have been careful to either give the halo no angular momentum, or to place the disk's symmetry axis along the angular momentum of the halo since otherwise additional evolution would result (Debattista & Sellwood 1999). Our model halo A was generated by the head-on merger of two prolate halos, themselves the product of a binary merger of spherical systems. The first merger placed the concentration $c = 10$ halos 800 kpc apart approaching each other at 50 $\mathrm{km\,s^{-1}}$, while the second merger starts with the remnant at rest 400 kpc from an identical copy. The resulting halo is highly prolate with a mild triaxiality. Halo model B was produced by the merger of two spherical halos starting at rest 800 kpc apart. Both halo A and B consist of 4×10^6 particles. The outer particles are $\sim 18\times$ more massive in halo A and $\sim 5\times$ more massive in halo B. A large part of the segregation by particle mass persists after the mergers and the small radius regions are dominated by low mass particles. Figure 1 shows the particle segregation in the case of halo A. We used a softening parameter $\epsilon = 0.1$ kpc for all particles although we have verified that using a larger softening, $\epsilon = 1$ kpc, for the more massive species does not change our results. Our force resolution was chosen to be smaller than the vertical scale of the disk, thereby resolving short-range scattering forces.

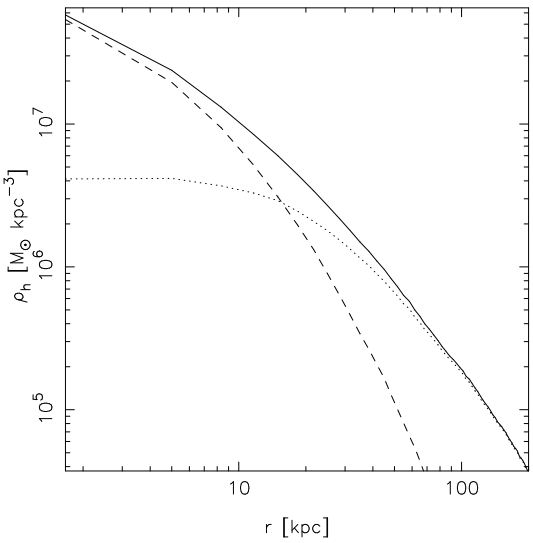

FIG. 1.— The spherically-averaged density distribution of dark matter particles in halo A before any baryonic mass is grown in the center. The solid line is the full density profile, the dashed line is for the lower mass species while the dotted line is for higher mass species.

Once we produced the prolate/triaxial halos, we inserted a disk of particles which remain rigid throughout the experiments. The disks are comprised of $300K$ equal-mass particles each with a softening $\epsilon = 60-100\,\mathrm{pc}$. The disk distribution was, in all cases, exponential with scale-length R_d and Gaussian scale-height $z_\mathrm{d}/R_\mathrm{d} = 0.05$. The disks were placed at various orientations within the halos. We refer to these experiments by the halo axis along which the disk's symmetry axis is aligned: in "short-

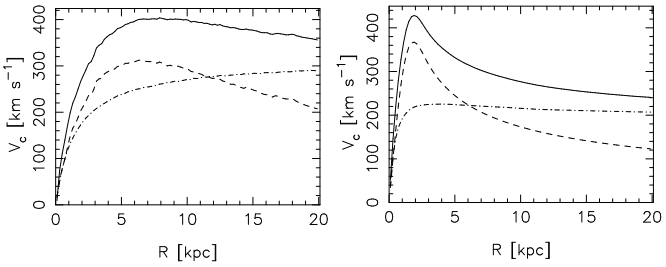

FIG. 2.— The azimuthally-averaged rotation curves of models SA1 (left) and P_lB1/P_fB2 (right) measured in the mid-plane. In both panels the solid line is the full rotation curve, the dashed line the contribution of the baryons and the dot-dashed line the contribution from the halo.

axis" (S) experiments, the symmetry axis of the disk is parallel to the short axis of the halo, while in "long-axis" (L) experiments, the symmetry axis of the disk is along the halo's major axis. If the halo is triaxial, then an "intermediate-axis" (I) experiment has the disk minor axis parallel with the halo's intermediate axis. Initially the disk has negligible mass but this grows adiabatically linearly over time to a mass M_b during a time t_g. After this time, we slowly evaporated it during a time t_e. Thus:

$$M_{disk}(t) = \begin{cases} M_b \ \frac{t}{t_g} & 0 \le t \le t_g \\ M_b \ (1 - \frac{t-t_g}{t_e}) & t_g \le t \le t_g + t_e. \end{cases} \quad (1)$$

During this time, the halo particles are free to move and achieve equilibrium with the disk as its mass changes. However all disk particles are frozen in place; in order to test whether motions of the baryonic particles affect the evolution, we also present experiments in which one or a few softened particles were introduced, with a mass grown in the same way. We refer to these experiments by the label "P" subscripted by "f" for growing particles frozen in place and by "l" for live particles free to move.

Run	Halo	r_{200} [kpc]	M_{200} [10^{12} M$_\odot$]	M_b [10^{11} M$_\odot$]	$R_{\rm d}$ [kpc]	t_g [Gyr]	t_e [Gyr]
SA1	A	215	4.5	1.75	3.0	5	2.5
SA2	A	215	4.5	5.25	3.0	5	2.5
SA3	A	215	4.5	1.75	1.5	5	2.5
IA1	A	215	4.5	1.75	3.0	5	2.5
LA1	A	215	4.5	1.75	3.0	5	2.5
LB1	B	106	0.65	1.05	3.0	15	7.0
P_lA1	A	215	4.5	1.75	0.5	5	2.5
P_lA2	A	215	4.5	0.87	0.5	2.5	2.5
P_lA3	A	215	4.5	1.75	5.0	5	2.5
P_lB1	B	106	0.65	0.7	3.0	10	4
P_fB2	B	106	0.65	0.7	3.0	10	4
P_lB3	B	106	0.65	0.35	0.1	5	5

TABLE 1
THE SIMULATIONS IN THIS PAPER. FOR THE PARTICLE SIMULATIONS, $R_{\rm d}$ REFERS TO THE SOFTENING OF THE PARTICLE(S). FOR RUNS P_lA1 AND P_lA2, THE VALUE OF M_b REFERS TO THE COMBINED MASS OF ALL THE SATELLITE PARTICLES AT t_g.

The basis of this work is that box orbit destruction is an irreversible process. Although classical mechanics are time-reversible, the random phases of any scattered orbits ensure that simply evaporating the central mass is not enough to return to the initial configuration. This would only be possible if we had a perfect integrator and if all velocities were reversed, which we do not do. Thus if we recover (nearly) the same distribution at $t_g + t_e$ as we started out with at $t = 0$ then scattering and chaos cannot have played a significant role in the shape evolution.

All the simulations in this paper were evolved with PKDGRAV (Stadel 2001), an efficient, multi-stepping, parallel treecode.

2.1. *Measuring halo shapes*

To measure the axis ratios c/a and b/a we adopt a method based on Katz (1991) which uses the eigenvalues of the (unweighted) moment of inertia tensor I. For each bin of N particles we computed I_{ij} as follows:

$$I_{ij} = \frac{\sum_{k=1}^{N} m_k r_{i,k} r_{j,k}}{\sum_{k=1}^{N} m_k}. \quad (2)$$

We then diagonalize I and calculate

$$b/a = \sqrt{\mathcal{I}_{22}/\mathcal{I}_{11}} \quad \text{and} \quad c/a = \sqrt{\mathcal{I}_{33}/\mathcal{I}_{11}}, \quad (3)$$

where the $\mathcal{I}_{ii}$'s are the eigenvalues of I and $\mathcal{I}_{11} \ge \mathcal{I}_{22} \ge \mathcal{I}_{33}$.

We measured shapes in shells of fixed semi-major axis widths around the center of the system. Thus these shape measurements are differential, rather than integrated (*cf.* Katz 1991). We use the iterative procedure of Katz (1991) in which the convergence criterion is a variation in axis ratios by $< 0.01\%$. In each iteration the semi-major axis of the shell is held fixed; a particle is included in the calculation of I_{ij} if $q_{lo} < q < q_{hi}$, where q is the ellipsoidal radius defined as

$$q^2 = x^2 + \left(\frac{y}{b/a}\right)^2 + \left(\frac{z}{c/a}\right)^2. \quad (4)$$

We used shell widths $q_{hi} - q_{lo} = 5$ kpc for all models.

The center of the system is taken to be the center-of-mass of a 1 kpc spherical shell about the potential minimum of the system, and is fixed for all shells. Tests performed in which the center-of-mass was allowed to vary by up to 0.5 kpc show less than 5% variation in the axis ratios past 10 kpc. Tests in which the limits of each shell were reduced by half around the average radius of that shell gave axis ratios which varied from the full resolution results by up to 10% in the worst cases and by less than 5% for most runs. In a few cases the density distribution within 5 kpc of the center is such that convergence is not reached after 20 iterations, or the axis ratios varied by as much as 20%. In these cases the number of particles in the central shell was less than $10K$, so we take this number to be a reasonable cutoff for the reliability of these innermost shells. This occurs in only 2 cases, and in general most inner shells have $> 25K$ particles, which we find to be more than enough to ensure consistent measurements with our method.

A useful parameter for expressing shape is the triaxiality parameter $T = (a^2 - b^2)/(a^2 - c^2)$ (Franx et al. 1991). The cases $T = 0$ and $T = 1$ correspond to oblate and prolate shapes respectively, while $T = 0.5$ is the maximally triaxial case.

3. RESULTS

3.1. *Short- and Intermediate-Axis Experiments*

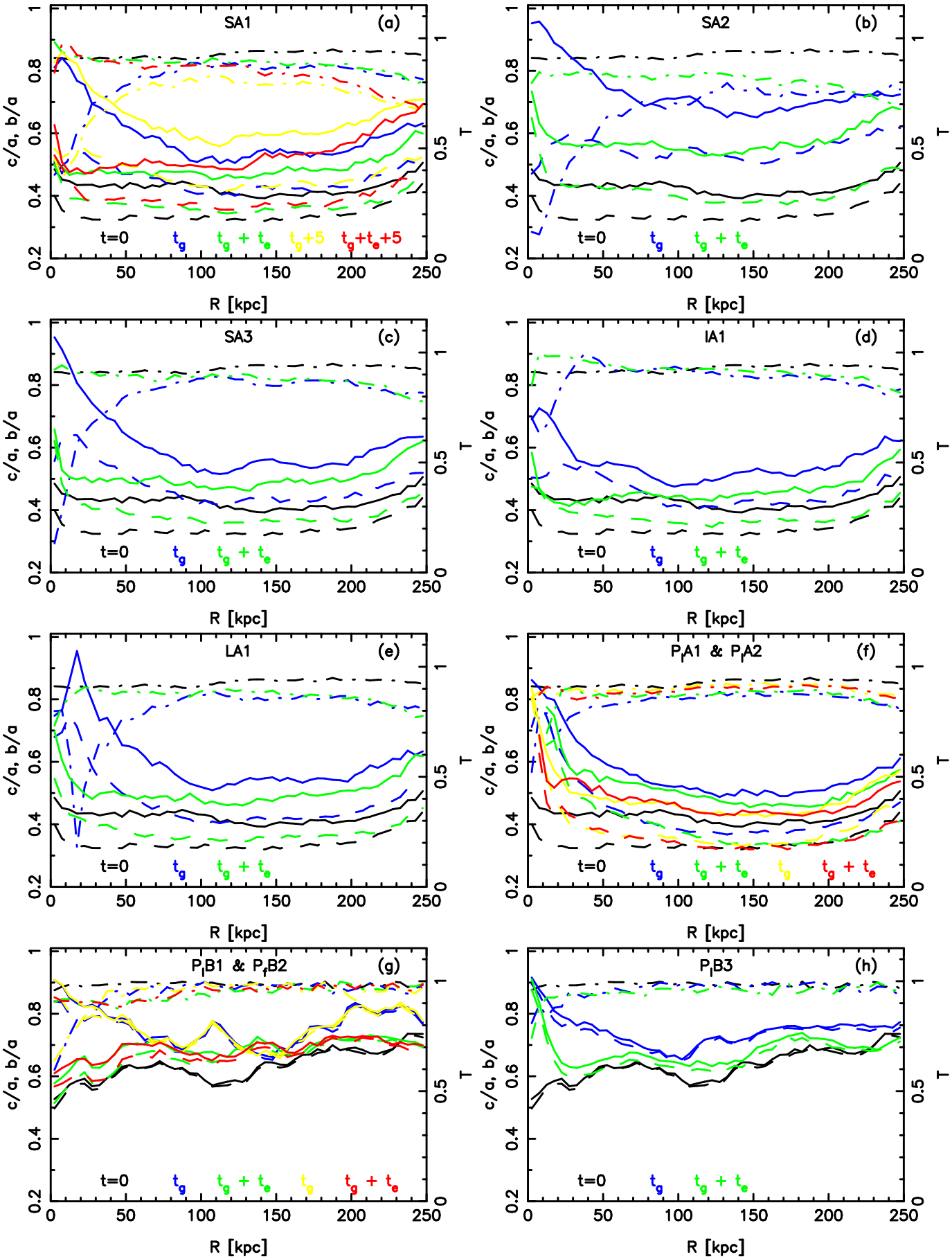

FIG. 3.— Shape evolution in runs (a) SA1, (b) SA2, (c) SA3, (d) IA1, (e) LA1, (f) P_lA1 and P_lA2, (g) P_lB1 and P_fB2 and (h) P_lB3. The solid lines show b/a, the dashed lines show c/a and the dot-dashed lines show T (with scale indicated on the right hand side of each

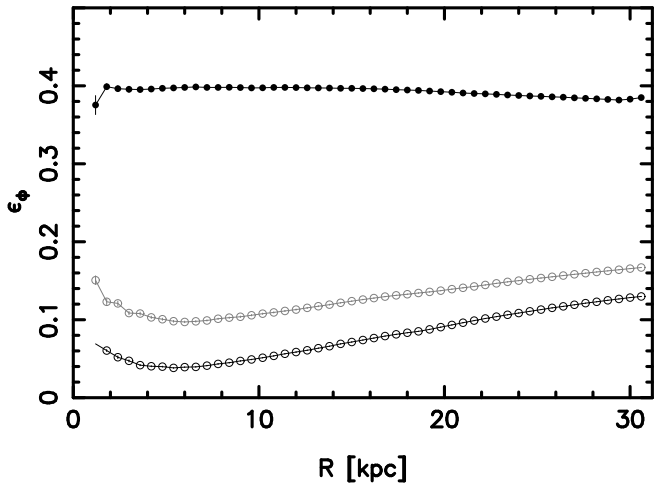

FIG. 4.— The ellipticity of the potential, ϵ_Φ, in the disk midplane in run SA1. The solid points are at $t = 0$, and the open points are at t_g, with gray for halo only and black for disk+halo.

In run SA1 we grew a disk inside halo A with the minor axes of the disk and halo aligned. This orientation is a natural one for disks to form in since simulations show that the angular momenta of halos are aligned with their *minor* axes (*e.g.* Warren et al. 1992; Porciani et al. 2002; Faltenbacher et al. 2005). Once the disk is grown to its full mass it dominates the inner rotation curve (see the left panel of Figure 2). The evolution of this highly prolate, mildly triaxial halo is shown in Figure 3a. The effect on the shape of the halo is large: it becomes much rounder in the plane of the disk ($b/a \gtrsim 0.6$ to 40 kpc, *i.e.* $\sim 0.2\ r_{200}$), as shown by the blue lines. The change in shape perpendicular to the disk is more modest and the inner halo becomes significantly more triaxial than it started out. In the disk plane, the combined potential becomes quite round, with $\epsilon_\Phi < 0.1$ to more than $6R_{\rm d}$ (Figure 4). However, once the disk is evaporated, the resulting halo shape, shown by the green lines in Figure 3a, is very similar to its original shape, with the net increase in both b/a and c/a being $\lesssim 0.1$ throughout the inner 100 kpc. The final triaxiality is barely changed from the starting one, despite the fact that the inner halo was almost maximally triaxial when the disk was at full mass.

Likewise, the final density and anisotropy of the system, shown in Figure 5, are not significantly changed by disk growth and evaporation, despite the factor of ~ 3.7 increase in halo central density at t_g. Further evidence that the orbital character of the halo is not substantially changed comes from the kinematics. The anisotropy of the halo, $\beta = 1 - \sigma_t^2/\sigma_r^2$, where $\sigma_t^2 = \frac{1}{2}(\sigma_\theta^2 + \sigma_\phi^2)$, is unchanged at $t = t_g + t_e$ whereas if box orbits had been destroyed to any significant extent we would have expected to see an increase in tangential anisotropy (e.g. Holley-Bockelmann et al. 2002).

Figure 3a (yellow and red lines) also shows the evolution when we left the disk at full mass for 5 Gyr before evaporating it. The halo becomes slightly rounder at all radii both after the additional 5 Gyr and once the disk is evaporated. The difference is largest inside ~ 30 kpc where the final b/a and c/a are about 0.1 larger at the end of the simulation. If scattering (whether physical or numerical) drives a large shape evolution then maintaining the disk at full mass will result in a larger irreversible shape change since the disk will have had a longer time to alter the orbital structure. However the fact that the difference between these two runs is so much smaller than between $t = 0$ and t_g implies that most of the halo shape change is due to orbit deformation, rather than scattering.

Model SA1 had a disk with $R_{\rm d} = 3$ kpc and with a baryon-to-dark matter fraction, $f_b = 0.039$, consistent with estimates for local galaxies (Jimenez et al. 2003). A more massive galaxy or a more compact one may lead to a less adiabatic halo shape change. We explored to what extent larger f_b or smaller $R_{\rm d}$ affect the halo shape in two further simulations. Run SA2 increased M_b by a factor of 3, while keeping $R_{\rm d}$ fixed. In this case the halo shape changed significantly all the way out to r_{200} after the disk is evaporated. Nevertheless, it remains quite prolate, with $b/a < 0.6$ and $c/a < 0.5$ as can be seen in Figure 3b. In contrast, at t_g the halo has $0.5 < b/a < 1.0$ within the inner 50 kpc. Even with this high $f_b \simeq 0.12$, or $\sim 70\%$ of the full cosmic baryon fraction (Spergel & et al. 2006), the irreversible change to the halo shape is $\lesssim 50\%$ of the full change at t_g out to 100 kpc. Run SA3 instead set $R_{\rm d} = 1.5$ kpc, keeping the ratio $z_{\rm d}/R_{\rm d}$ fixed (and decreasing all softenings appropriately). The evolution in this case is shown in Figure 3c; as in run SA1, although the halo at $t = t_g$ is substantially rounder than at the start, after the disk is evaporated the halo recovers most of its original shape. Of runs SA2 and SA3, making the disk more massive (SA2) had a larger effect on the final shape than did making it more compact.

Run IA1 explored whether having the disk orthogonal to the intermediate axis makes a significant difference to the final shape, with all other parameters as in run SA1. The resulting shape evolution is presented in Figure 3d. In this simulation the halo remained more elongated than in run SA1 despite having the same M_b. The axis ratios of the halo at t_g cross over at ~ 30 kpc, where the halo's flattening orthogonal to the disk causes the minor axis to switch from the disk plane to the orthogonal direction. Once the disk is evaporated, the halo ends very nearly axisymmetric in cross-section in this inner region but continues to be highly prolate. As in run SA1, the net change in halo shape is relatively small at $t = t_g + t_e$.

3.2. *Long-Axis Experiments*

In run LA1 we placed the disk with its symmetry axis along the long axis of the halo. This orientation has been suggested to be favored by the distribution of satellites around the Milky Way (Zentner et al. 2005) and by the Sagittarius dwarf tidal stream (Helmi (2004) but see also Fellhauer et al. (2006)). Other than the disk's orientation, the parameters of this experiment are identical to those of run SA1. As in that experiment, the halo in run LA1 is significantly deformed by the growing disk, but it recovers its shape nearly completely once the disk is evaporated, as shown in Figure 3e. Likewise, the spherically averaged kinematic evolution of run LA1 is indistinguishable from that of SA1, as seen in Figure 5.

A unique characteristic of the evolution in long-axis experiments is their tendency for the major axis of the inner halo to switch orientation by 90° into the disk plane once the disk grows sufficiently massive. For run LA1 this is evident in Figure 3e, which shows that the halo is spher-

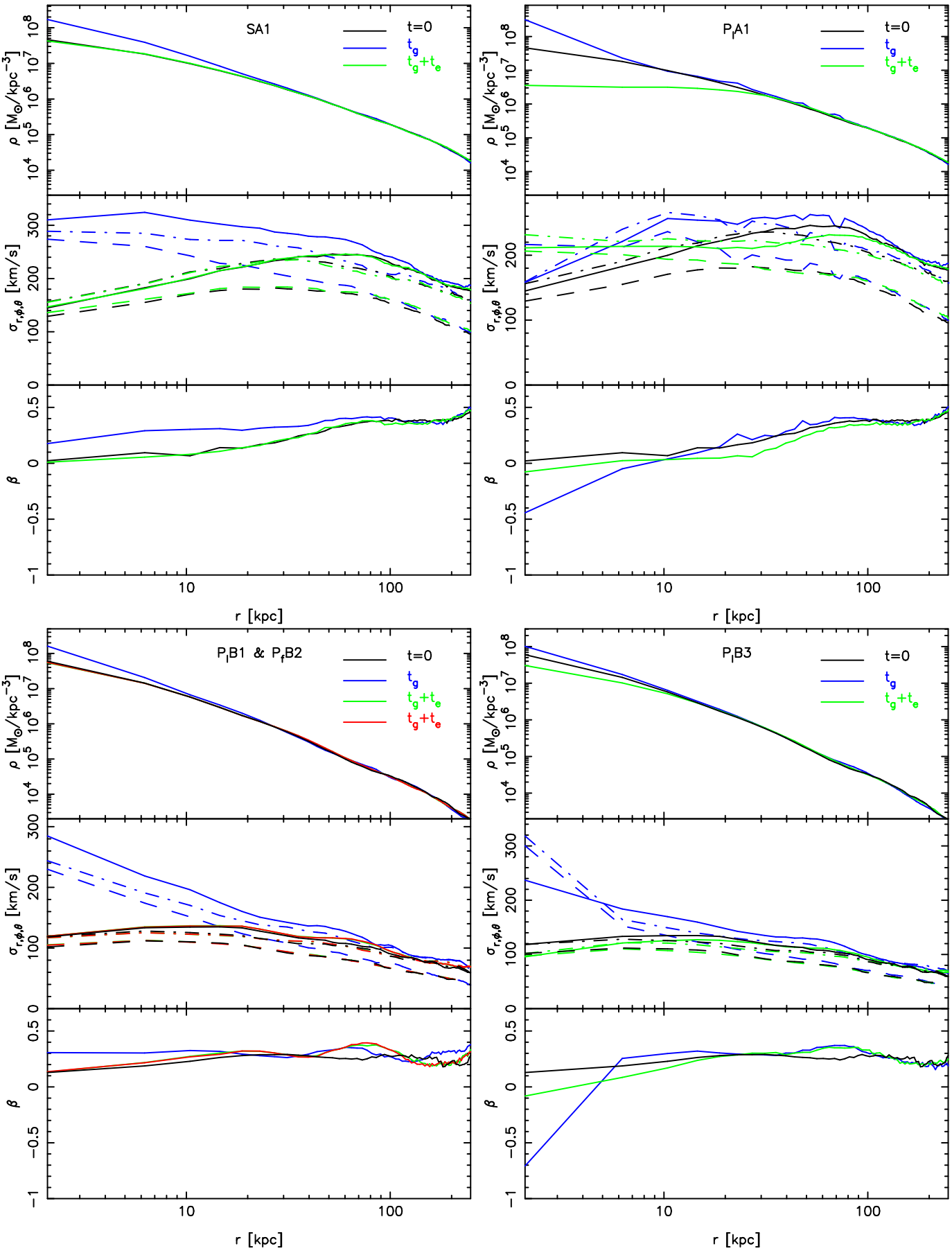

FIG. 5.— The evolution of the spherically averaged density and kinematic properties in runs SA1 (top-left), P_lA1 (top-right), P_lB1 and P_fB2 (bottom left) and P_lB3 (bottom right). The black, blue and green lines correspond to $t = 0$, t_g and $t_g + t_e$. The red lines show $t_g + t_e$ for P_sB2. The top panels shows the densities. In the middle panels the solid lines indicate σ_r, the dashed lines σ_ϕ and the dot-dashed lines

ical at ~ 10 kpc but is quite prolate-triaxial at smaller radii. But this behavior is better illustrated with the more nearly axisymmetric halo B. In run LB1, as M_{disk} increases, shells of the prolate inner halo become spherically symmetric; further increase in M_{disk} then leads to the shell becoming not only flatter vertically but also acquiring an *elongation* with its major axis in the plane of the disk, *i.e.* the symmetry axis of the inner halo flips by 90° and becomes orthogonal to that of the outer halo (see Figures 6 and 7). The direction along which this reorientation occurs is not random since the halo is initially not perfectly axisymmetric on large scales. Continued increase in M_{disk} causes the symmetry axis to flip orientation to larger radii eventually saturating at about 10 kpc. The halo orientation flips do not occur when the disk is replaced by point particle. The dotted gray line in Figure 7 shows the orientation of the major axis in run P$_l$B1, at a time when its mass is the same as that in LB1; no flip in the major axis direction can be seen.

3.3. *Softened Point Masses*

The experiments described above all had rigid disks frozen in place. While we have been careful to recenter the halo in position and velocity after the mergers and before growing the disks, some residual relative motion of the inner and outer parts of the halos remained. This motion is damped as the mass of the fixed disk increases, possibly causing some change in the halo shapes. In order to test for artifacts associated with such damping, we performed a number of experiments using point particles only, in which case it is possible to allow the growing particles to move. By comparing two such experiments, in one of which the growing particle is free to move (P$_l$B1) while being fixed in place in the second (P$_f$B2) we are able to assess the effect of fixing the disk in place. The rotation curve at t_g is shown in Figure 2. In both cases, the shape is largely recovered at $t_g + t_e$ (Figure 3g). But P$_l$B1 is very slightly rounder inside 10 kpc than is P$_f$B2 compared with the initial halo. Thus, rather than enhancing the sphericalization of the halo, fixing the growing massive particles in place has the opposite effect. Thus our use of fixed disks should not have induced an artificial shape change.

In runs P$_l$B1 and P$_f$B2 the growing particle had a softening of $\epsilon = 3$ kpc, a reasonable size for a galaxy. In run P$_l$B3 we decreased the softening length of the particle to 100 pc. Even though M_b in this experiment was half of that in runs P$_l$B1 and P$_f$B2, the final halo after $t_g + t_e$ remains substantially rounder interior to 20 kpc than in those runs (but is largely recovered at larger radii). Treating the central particle as though it were a black hole, its sphere of influence assuming $\sigma_0 = 100\,\mathrm{km\,s^{-1}}$ from $t = 0$, is ~ 15 kpc. This is comparable to the radius out to which the particle irreversibly alters the shape of the halo. Likewise, the halo mass within 20 kpc is comparable to that in the central particle: at $t = 0$, the halo mass within this radius is $4M_b$. In the inner ~ 5 kpc the halo shape does not change significantly between t_g and $t_g + t_e$. Despite the different final state, Figure 3h also shows that the halo shape at t_g is not much different from that in P$_l$B1 and P$_f$B2.

Figure 5 plots the kinematics of runs P$_l$B1, P$_f$B2 and P$_l$B3. While the evolution of density and kinematics is largely reversible in runs P$_l$B1 and P$_f$B2, this is not the case in run P$_l$B3 and the system becomes significantly tangentially biased, as expected if box orbits are destroyed.

Whereas run SA3 with $R_\mathrm{d} = 1.5$ kpc, which is not unreasonably small for most galaxies, did not significantly cause box orbit destruction, the $\sim 10\times$ more centrally concentrated run P$_l$B3 is able to cause a large irreversible change to the halo shape out to $\sim 0.3\ r_{200}$. However this scale is unrealistically small for most galaxies.

3.4. *Condensation onto Satellite Substructures*

The comparison of runs P$_l$B1 and P$_f$B2 suggested that allowing baryonic particles to move leads to a larger irreversible change in halo shapes. In our final set of models, P$_l$A1 and P$_l$A2, we explore the effects of baryons cooling inside substructures orbiting within the halo, rather than directly onto a central massive object. The presence of copious substructure is one of the main predictions of CDM (Moore et al. 1999; Klypin et al. 1999; Ghigna et al. 2000). A concern which arises is whether these dark substructures are dynamically important for the evolution of the host. For example the ability of substructure to vertically heat disks has been explored (Moore et al. 1999; Font et al. 2001).

In order to explore the effects of baryons cooling onto substructures, we started with the halo A, selecting 10 particles which stay within 200 kpc but otherwise at random, and linearly increased each of their masses to give the same total baryonic mass as in run SA1, and with $\epsilon = 0.5$ kpc for each satellite. We grew to full mass and then evaporated these satellites; because they were allowed to move, they also lost angular momentum to the halo and started sinking. Of the 10 satellites, only one remains at $r > 50$ kpc, the rest having fallen to $R < 25$ kpc by the end of the simulation. Thus the evolution of these experiments is inherently irreversible. Furthermore, these experiments used softened point particles to represent satellites, and so cannot be tidally stripped. Therefore the effects of these substructures are maximal and would be smaller in nature.

The evolution of the shape in these two models is presented in Figure 3f. After the particles reach their full mass, the halo of run P$_l$A1 is about as round as in run SA1. However, the halo does not recover much of its original shape after the particles are evaporated. Clearly this is a case where the density distribution of the halo has been altered to a large extent. In run P$_l$A2, when the massive particles were evaporated after reaching only half the mass of run P$_l$A1, the halo again stayed rounder than in earlier runs. Figure 5 shows that angular momentum transferred by baryons to the halo can erase the cusp, in agreement with previous results (Tonini et al. 2006; Mashchenko et al. 2006; Read et al. 2006; Weinberg & Katz 2007) although the contraction caused by the growing central mass masks the core. The fact that the shape at t_g of models SA1 and P$_l$A1 is so similar, although the former retains most of its phase space structure whereas the latter is strongly changed, suggests that the change in halo shape between $t = 0$ and t_g is mostly driven by the change in the potential, rather than by scattering. Run P$_l$A3 was identical to P$_l$A1 but used a $10\times$ larger softening for the satellite particles. In this case the final halo shape at $t_g + t_e$ was rather similar to that in P$_l$A1 whereas the shape at t_g

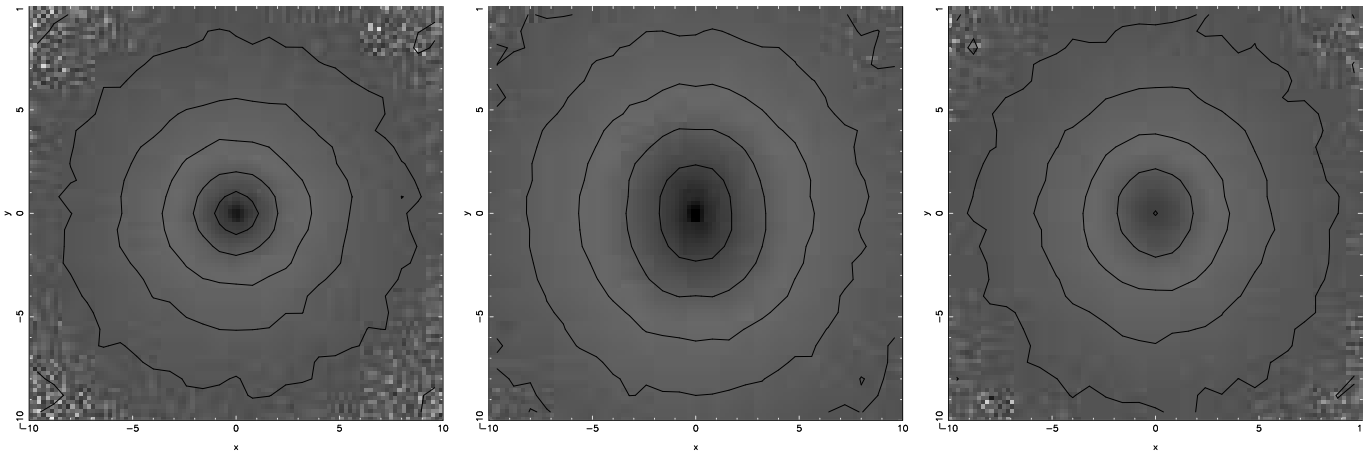

FIG. 6.— The evolution of the halo in run LB1. The halo is seen in cross-section in the plane of the disk, with only the region $|z| < 5$ kpc shown, where the z-axis is the symmetry axis of the disk and of the halo. The panels show $t = 0$ (left), t_g (middle) and $t_g + t_e$ (right). The halo is initially axisymmetric, becomes elongated orthogonal to the symmetry axis at small radii at t_g and largely recovers its axisymmetry at $t_g + t_e$.

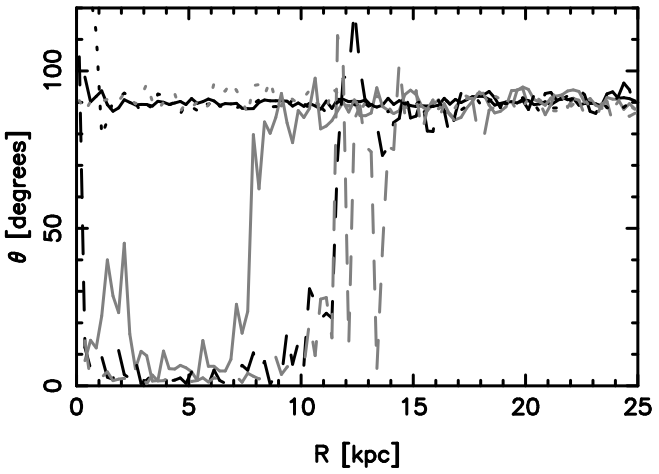

FIG. 7.— The major axis orientation at different times in run LB1. The solid black and gray lines are at $t = 0$ and $t_g/3$, the dashed black and gray lines are at $2t_g/3$ and t_g and the black dotted line is at $t_g + t_e$. The gray dotted line shows run P_lB1 at t_g.

was more elongated by $b/a \sim 0.1$. The larger softening at the center from the fallen satellites accounts for the more elongated shape at t_g whereas the roughly equal angular momentum gained by the two halos at $t_g + t_e$ accounts for the very similar shapes at that point.

Substructure, even if purely dark matter, may also lead to a change in halo shape if they excite oscillations of the central baryonic mass. Although we have not run simulations to test this, it is likely that this effect is important only so long as the mass of the substructure is comparable to that of the central baryonic mass.

4. ORBITAL EVOLUTION

We explored the evolution of the orbital character of the models by considering a subsample of 1000 particles in run SA1 and exploring their orbits at various points in the simulation. The 1000 particles were randomly chosen from the $t = 0$ distribution such that they were inside $r = 200$ kpc. We then integrated their motion as test particles while holding all the other particles fixed in place. We used a fixed timestep of 0.1 Myr and integrated for 15 Gyrs, storing the phase space coordinates of each test particle every 1 Myr. For the same 1000 particles, we carried out this operation at $t = 0$, t_g, and $t_g + t_e$. Note that because we freeze the background potential, in effect what we are doing is computing the orbits of the particles at $t = 0$, t_g, and $t_g + t_e$. The fact that we integrated for 15 Gyrs only ensures that we have sufficient points on each orbit to properly characterize each orbit (which we will do elsewhere). In this paper we present only a preliminary analysis of these data, demonstrating with a few examples that a good number of box-like orbits at $t = 0$ return to very similar box-like orbits at $t_g + t_e$. We do this by presenting their configuration space projection at each of the 3 different times. Such an analysis cannot distinguish between box orbits and mildly chaotic, elongated orbits but this is unimportant anyway for our present purposes since we have integrated for over a Hubble time so if they are mildly chaotic they can still support a triaxial halo. A full analysis of the orbital structure of these models using more sophisticated techniques will be presented elsewhere.

Of the 1000 orbits, we start by presenting 9 particles which, at $t = 0$, (1) remain inside 25 kpc, (2) do not have a fixed sense of rotation relative to any of the three major axes, (3) reach a radius of at least 10 kpc and (4) get within 0.2 kpc of the center. The evolution of many of the other 991 orbits is qualitatively similar to that of the 9 presented here. Figure 8 projects the 9 orbits onto the halo symmetry planes, where the x-axis is the halo's major axis and the z-axis is the disk's symmetry axis. Most orbits at $t_g + t_e$ are quite similar to what they looked like at $t = 0$. None of the orbits seem strongly chaotic, either at t_g or at $t_g + t_e$, although they may be weakly chaotic. Moreover, most orbits retain a box-like shape at t_g, but have a significantly rounder shape than at $t = 0$. At t_g, three of the initially box-like orbits become round (those labelled 'a', 'f' and 'h'); of these orbit 'h' changes character completely, becoming a loop orbit. Some of the orbits have a slight banana shape; in the full sample of orbits we found many cases of strongly banana-shaped orbits. These had a tendency to become more planar but are still distinctly elongated at $t_g + t_e$. In a few cases we also found the opposite occurring — slightly banana

orbits becoming more strongly bent — but this was less common. Of the box-like orbits in Figure 8 some are rounder in the (x, y) plane at $t_g + t_e$ (*e.g.* those labelled 'a', 'f' and 'i'), but some are rounder at $t = 0$ (*e.g.* 'c' and 'e'), suggesting that differences in shape are due to (possibly numerical) scattering.

We quantify the shape change of individual orbits by plotting, in Figure 9, σ_y/σ_x, where $\sigma_x^2 = \sum_t x_t^2$ and similarly for σ_y^2 and the sum is over timesteps. The significantly rounder shape of orbits at t_g compared to $t = 0$ is apparent, with the vast majority of orbits initially aligned with the halo having larger σ_y/σ_x at the later time. Orbits initially elongated along the halo's minor axis, as well as orbits initially rounder than $\sigma_y/\sigma_x \gtrsim 0.6$ end up round, with $\sigma_y/\sigma_x \simeq 1$. Instead at $t_g + t_e$ the orbits tend to return to their initial elongation, especially for the most elongated orbits. The right panel shows the distribution of σ_y/σ_x; orbits become substantially rounder at t_g but the population as a whole recovers the original distribution to a large extent once the disk is evaporated.

A comparison of orbital evolution in runs $\mathrm{P}_f\mathrm{B2}$ and $\mathrm{P}_l\mathrm{B3}$ provides a good example of strong chaos radically altering the shape of triaxial halos. Other than in the satellite simulations, only the very centrally concentrated run $\mathrm{P}_l\mathrm{B3}$ resulted in a large irreversible halo shape change. We again selected 1000 orbits from particles within the inner 200 kpc of halo B at $t = 0$. We integrated their orbits as above; for $\mathrm{P}_f\mathrm{B2}$ we use $t_g/2$ when the central particle has the same mass as at t_g in model $\mathrm{P}_l\mathrm{B3}$. Although we are comparing the two models at the same mass, the orbits at time $t_g + t_e$ in model $\mathrm{P}_f\mathrm{B2}$ were computed after the central particle was evaporated from a mass twice that reached in $\mathrm{P}_l\mathrm{B3}$. As before, we present in Figure 10 nine orbits which at $t = 0$ are box-like. It is clear that these box-like orbits in $\mathrm{P}_l\mathrm{B3}$ are more significantly scattered than in run $\mathrm{P}_f\mathrm{B2}$. In model $\mathrm{P}_f\mathrm{B2}$, only one orbit (labelled 'f') appears to have changed substantially at the end of the simulation, while orbits 'a' and 'd' become fish orbits (although the original orbits may have been librating about fish orbits). Orbit 'b' is largely unchanged and the remaining orbits are all box-like. In model $\mathrm{P}_l\mathrm{B3}$, orbit 'e' is changed about as much as orbit 'f' in $\mathrm{P}_f\mathrm{B2}$. However, 4 of the 9 orbits, 'f'-'i', are very strongly changed by $t_g + t_e$ and are no longer able to support a triaxial shape. Figure 11 compares the distribution of all 1000 particle and a clear depletion of elongated orbits is evident in $\mathrm{P}_l\mathrm{B3}$ compared with run $\mathrm{P}_f\mathrm{B2}$.

5. DISCUSSION

5.1. *Timesteps*

Besides the experiments described here, we have performed a number of tests of the numerics to verify that our results are robust. One of the main concerns for shape evolution is the timestep used. Shen & Sellwood (2004) found that too large timesteps result in bars being destroyed too easily, because orbits are no longer followed accurately near the central mass concentration. Our simulations were performed with multi-stepping. With a base timestep of Δt, particles move on timesteps $\Delta t/2^n$, where n is the rung level satisfying the condition $\delta t = \Delta t/2^n < \eta\sqrt{\epsilon/a}$, with ϵ the particle's softening, a is its acceleration and η a tolerance parameter. We used $\eta = 0.2$, a conservative value; with a base timestep $\Delta t = 5$ Myr simulation SA1 at t_g had a range of timesteps down to $5/2^5 = 0.16$ Myr. If instead we set $\eta = 2$ the timestep distribution only reaches to $5/2 = 2.5$ Myr. The effect of these larger timesteps, shown in Figure 12, is manifest at $r \lesssim 20$ kpc, which remains significantly rounder at $t_g + t_e$ than when $\eta = 0.2$. The quite modest net shape change in our simulations implies that the timesteps we used were sufficiently small to correctly follow the evolution near the center.

5.2. *Conclusions*

We have demonstrated that the substantial axisymmetrization caused by a disk growing inside a dark matter halo is to a large extent, though not wholly, reversible. Macciò et al. (2007) have recently argued that box orbits become chaotic as the disk grows inside a triaxial halo, leading to the rounder shape. The main difficulty with this interpretation is that as the disk is evaporated, box orbits have to become repopulated in order that the halo recovers its original shape. Apart from being unlikely for such a highly ordered system as a triaxial halo, this interpretation is not supported by our orbital analysis, which shows that box-like orbits become significantly rounder when the disk is grown but nevertheless remain elongated. Moreover, a large fraction of individual particles return to very nearly the same elongated orbits as they started out with. This makes it implausible that the shape change is due to a large increase in strong chaos in the orbits. Instead we find that the disks that form are simply not concentrated enough to lead to substantial chaos. Likewise, in their analysis of the effects of black holes in triaxial elliptical galaxies, Holley-Bockelmann et al. (2002) found that chaos is associated with the black hole only, not with the stellar cusp which forms as the black hole grows. Presumably a stellar cusp is not concentrated enough to scatter orbits and destroy triaxiality efficiently. This need not mean, however, that chaos is not enhanced by the presence of the disk. It could well be that orbits are becoming weakly chaotic but do not diffuse sufficiently on a Hubble timescale to significantly weaken triaxiality. This interpretation is consistent with the orbital characterization of Macciò et al. (2007) but does not support the claim that the shape change is largely due to enhanced chaos.

The most plausible explanation for the shape change, consistent with the orbits presented above, is that orbits (whether regular or chaotic) merely become rounder as the disk grows. In this case, evaporating the disk would recover exactly the same configuration. This explanation is also supported by the much smaller effects of scattering when it can be deduced that scattering has occurred, which happens twice. In the first instance, we showed that keeping the disk at full mass for 5 Gyrs before evaporating it only caused a small additional change in the final halo shape, implying that scattering is only responsible for a small part of the shape change. The second case comes from the comparison of runs $\mathrm{P}_l\mathrm{B1}$ and $\mathrm{P}_l\mathrm{B3}$, where we find that the halo shape at t_g is rather similar, despite the fact that in run $\mathrm{P}_l\mathrm{B3}$ box orbits are significantly destroyed. These two examples directly illustrate that box orbit destruction is a much smaller factor in the change in shape of the halo than is simple orbit defor-

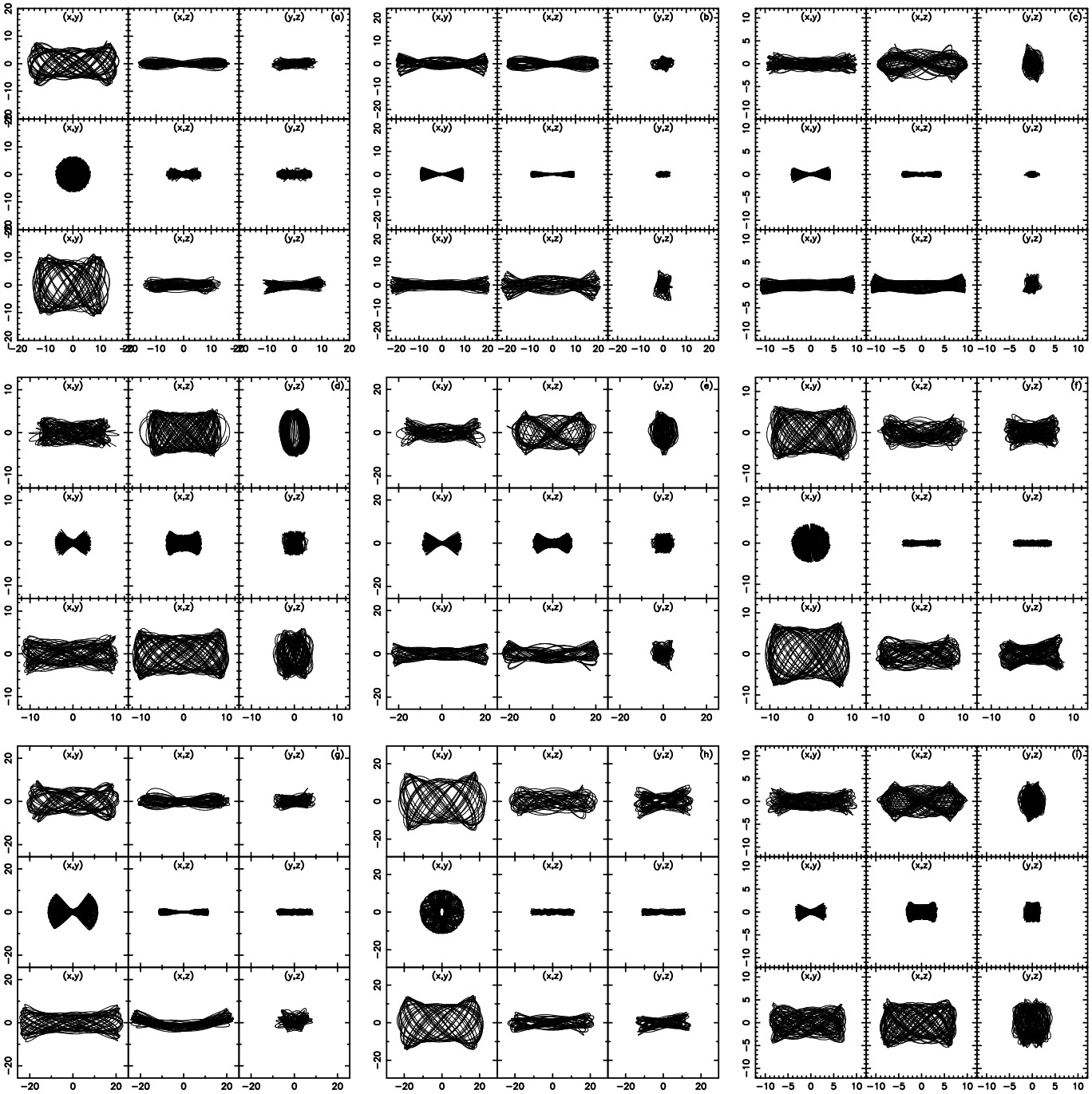

FIG. 8.— A sample of initially box-like orbits in run SA1. In each set of panels, the top row is at $t = 0$, the middle row is at t_g and the bottom row is at $t_g + t_e$; from left to right the panels show projections onto the (x, y), (x, z) and (y, z) planes. Each orbit has been integrated for 15 Gyr from each of $t = 0$, t_g and $t_g + t_e$.

mation.

If baryons instead cool onto substructures within the halo then its triaxiality is very efficiently destroyed. Since the evolution of disks can be strongly influenced by halo triaxiality (*e.g.* Ideta & Hozumi 2000), any process which artificially reduces triaxiality can lead to biases in the properties of galaxies forming in cosmological simulations. Agertz et al. (2006) demonstrate that the evolution of gas blobs in smoothed particle hydrodynamics (SPH) simulations is different from that found in Eulerian gas codes. They interpreted this difference as being due to the unphysically poor mixing of traditional SPH, which allows blobs to survive longer in SPH. In nature, baryonic cooling inside substructures is strongly suppressed by feedback from supernovae (Dekel & Silk 1986; Governato et al. 2004, 2007). Moreover satellites in cosmological simulations tend to have denser, more concentrated gas components than their real counterparts, which makes them harder to strip by ram pressure and tides (Mayer et al. 2007), and thus likely to artificially enhance halo shape changes. If feedback is not properly included and resolution is not sufficiently high in simulations, then baryons cooling inside substructures may bias the global evolution of simulated galaxies. Com-

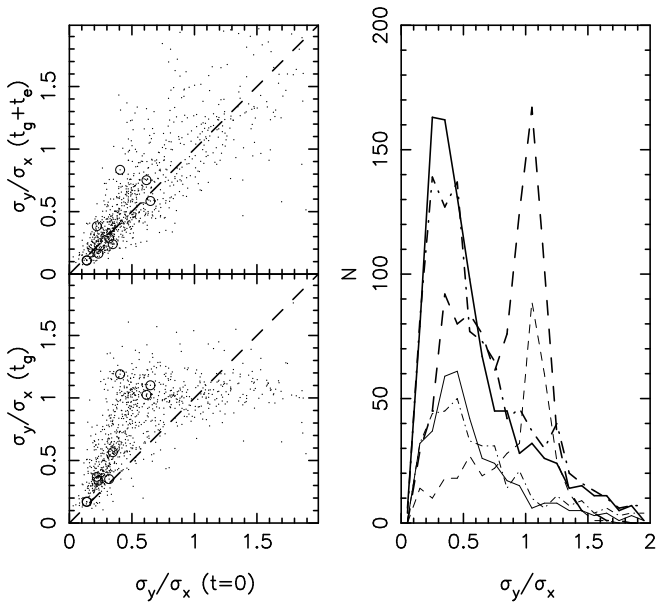

FIG. 9.— The shape transformation of orbits in run SA1. In the left panels, the dashed line shows the diagonal. The circled points are for the nine particles of Figure 8. In the right panel, the solid, dashed and dot-dashed lines show the distributions at $t = 0$, t_g and $t_g + t_e$, respectively. The thick lines are for the full distribution of 1000 particles, while the thin lines are for only those particles that remain inside $r = 50$ kpc at $t = 0$.

paring cosmological simulations of dark matter only and dark matter plus gasdynamics, Kazantzidis et al. (2004) found that the same halos which form are rounder than those forming in the absence of baryons out to the virial radius. Our simulations show that such shape variations may not have resulted from the destruction of box orbits. The main caveat to this conclusion is that dense blobs of cooled gas may become dense and massive enough in such simulations to irreversibly change the phase space distribution of the halo.

Since the changing halo shape is, to a large extent, reversible, it is likely that this evolution can be computed from appropriately defined adiabatic invariants. Such a calculation seems worth undertaking.

5.3. *Summary*

Our results can be summarized as follows:

1. The adiabatic growth of disks with realistic scalelengths and masses inside prolate/triaxial halos leads to a large change in the shape of the halo. Axis ratios can change by > 0.2 out to roughly $0.5\ r_{200}$. Even as it becomes rounder, anisotropic compression leads to a more triaxial halo inside $r = 25$ kpc. The growth of the disk drives the halo kinematics to larger radial anisotropy.

2. Despite these large changes, the shape is largely recovered when the disk is adiabatically evaporated. Likewise, the density profile and the kinematic structure is mostly recovered in this process. The total change in final halo structure is larger for more massive or more centrally concentrated disks, but is still a relatively small fraction of the total shape change when the disk is at full mass. As in the case of black holes at the centers of cuspy elliptical galaxies (Gerhard & Binney 1985; Holley-Bockelmann et al. 2002), the bulk of the irreversible halo shape change occurs in the inner region of the galaxy. Thus this small irreversible shape change is presumably driven by orbit scattering.

3. Large irreversible changes in halo shape require very centrally concentrated structures; in our simulations we found that we need scales of ~ 100 pc to accomplish this. Even then, the irreversible shape change was restricted to the inner $\sim 30\%$ of r_{200}.

4. Box orbit destruction cannot be the right interpretation for the difference in shape between before and after the disk is grown. Such a process is not reversible once the disk is evaporated but we found that a large fraction of box-like orbits individually return to very similar orbits to their starting ones after the disk is evaporated. Moreover, we find that orbits starting box-like become significantly rounder when the disk is at full mass, but retain their box-like character. Since chaotic orbits can still support a triaxial structure (Poon & Merritt 2002) it is possible that growing the disk leads to an increase in the fraction of mildly chaotic orbits.

5. When the disk minor axis and halo major axis are aligned, growth of the disk has a tendency to drive an elongation within the plane of the disk, even when the initial halo is very nearly axisymmetric.

6. If baryons condense onto substructures, instead of onto a central disk/spheroid, then a large irreversible change in halo shape occurs. However in this case the evolution is rendered irreversible by virtue of the baryons losing angular momentum to the halo and sinking to the center. Because of poor mixing in SPH (Agertz et al. 2006) or too highly concentrated satellites (Mayer et al. 2007), condensation of baryons onto satellites can significantly alter the shape of the halo and affect the subsequent evolution of the disk.

Acknowledgments.
This paper is based in part upon work supported by the National Science Foundation under the following NSF programs: Partnerships for Advanced Computational Infrastructure, Distributed Terascale Facility (DTF) and Terascale Extensions: Enhancements to the Extensible Terascale Facility. Many additional simulations were carried out at the University of Zürich on zBox and at the Arctic Region Supercomputing Center. V.P.D. thanks the University of Zürich for hospitality during part of this project. V.P.D. is supported by a Brooks Prize Fellowship in Astrophysics at the University of Washington and receives partial support from NSF ITR grant PHY-0205413. S.K. acknowledges support by the U.S. Department of Energy through a KIPAC Fellowship at Stanford University and the Stanford Linear Accelerator Center. We thank Andrea Macciò and Ioannis Sideris for fruitful discussions.

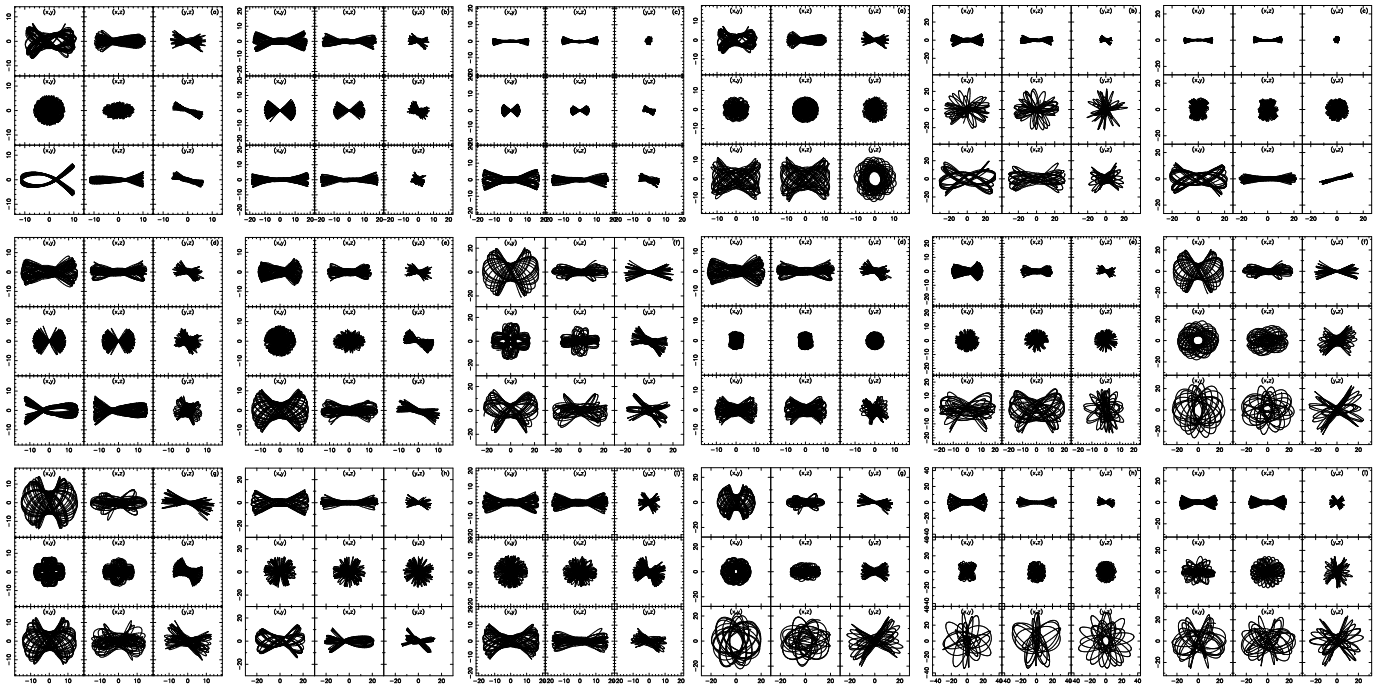

FIG. 10.— A sample of initially box-like orbits in run P_fB2 (left 3 columns) and P_lB3 (right 3 columns). Note that we show the evolution of the same 9 starting orbits in the two different models. In each set of panels, the top row is at $t = 0$, the middle row is at $t_g/2$ (P_fB2) or t_g (P_lB3) and the bottom row is at $t_g + t_e$; from left to right the panels show projections onto the (x, y), (x, z) and (y, z) planes. Each orbit has been integrated for 15 Gyr from each starting point.

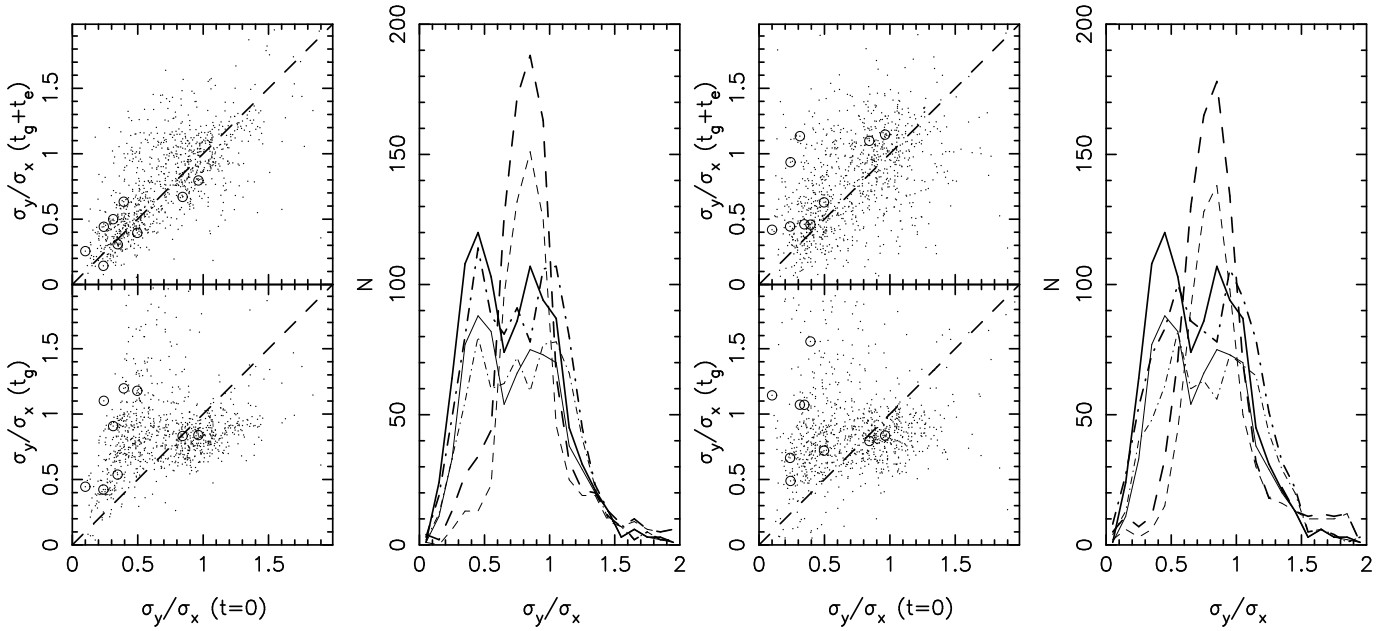

FIG. 11.— Identical to Figure 9 but for runs P_fB2 (left) and P_lB3 (right). The final distribution of orbits is significantly depleted of elongated orbits in run P_lB3 compared with run P_fB2.

REFERENCES

Agertz, O., et al. 2006, ArXiv Astrophysics e-prints

Allgood, B., Flores, R. A., Primack, J. R., Kravtsov, A. V., Wechsler, R. H., Faltenbacher, A., & Bullock, J. S. 2006, MNRAS, 367, 1781

Andersen, D. R., Bershady, M. A., Sparke, L. S., Gallagher, J. S., & Wilcots, E. M. 2001, ApJ, 551, L131

Bailin, J., & Steinmetz, M. 2005, ApJ, 627, 647

Bardeen, J. M., Bond, J. R., Kaiser, N., & Szalay, A. S. 1986, ApJ, 304, 15

Barnes, E. I., & Sellwood, J. A. 2003, AJ, 125, 1164

Barnes, J., & Efstathiou, G. 1987, ApJ, 319, 575

Bartelmann, M., Steinmetz, M., & Weiss, A. 1995, A&A, 297, 1

Buote, D. A., & Canizares, C. R. 1994, ApJ, 427, 86

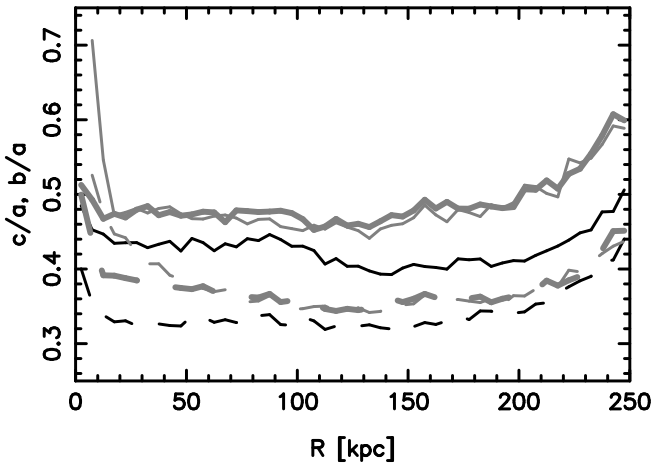

FIG. 12.— The effect of timestep size on the evolution of run SA1. The black lines shows the shape at $t = 0$ while the gray lines are for $t_g + t_e$, with the thick line the standard result with $\eta = 0.2$ and the thin lines for $\eta = 2$. As in Figure 3, the solid lines show b/a while the dashed lines show c/a. The larger timesteps lead to an evolution which is less reversible.

Buote, D. A., Jeltema, T. E., Canizares, C. R., & Garmire, G. P. 2002, ApJ, 577, 183
Debattista, V. P. 2003, MNRAS, 342, 1194
Debattista, V. P., Mayer, L., Carollo, C. M., Moore, B., Wadsley, J., & Quinn, T. 2006, ApJ, 645, 209
Debattista, V. P., & Sellwood, J. A. 1999, ApJ, 513, L107
Dekel, A., & Silk, J. 1986, ApJ, 303, 39
Dubinski, J. 1994, ApJ, 431, 617
Dubinski, J., & Carlberg, R. G. 1991, ApJ, 378, 496
Faltenbacher, A., Allgood, B., Gottlöber, S., Yepes, G., & Hoffman, Y. 2005, MNRAS, 362, 1099
Fellhauer, M., et al. 2006, ApJ, 651, 167
Font, A. S., Navarro, J. F., Stadel, J., & Quinn, T. 2001, ApJ, 563, L1
Franx, M., & de Zeeuw, T. 1992, ApJ, 392, L47
Franx, M., Illingworth, G., & de Zeeuw, T. 1991, ApJ, 383, 112
Franx, M., van Gorkom, J. H., & de Zeeuw, T. 1994, ApJ, 436, 642
Frenk, C. S., White, S. D. M., Davis, M., & Efstathiou, G. 1988, ApJ, 327, 507
Fridman, T., & Merritt, D. 1997, AJ, 114, 1479
Gerhard, O. E., & Binney, J. 1985, MNRAS, 216, 467
Ghigna, S., Moore, B., Governato, F., Lake, G., Quinn, T., & Stadel, J. 2000, ApJ, 544, 616
Governato, F., et al. 2004, ApJ, 607, 688
Governato, F., Willman, B., Mayer, L., Brooks, A., Stinson, G., Valenzuela, O., Wadsley, J., & Quinn, T. 2007, MNRAS, 374, 1479
Helmi, A. 2004, MNRAS, 351, 643
Holley-Bockelmann, K., Mihos, J. C., Sigurdsson, S., Hernquist, L., & Norman, C. 2002, ApJ, 567, 817
Huizinga, J. E., & van Albada, T. S. 1992, MNRAS, 254, 677
Ibata, R., Lewis, G. F., Irwin, M., Totten, E., & Quinn, T. 2001, ApJ, 551, 294
Ideta, M., & Hozumi, S. 2000, ApJ, 535, L91
Iodice, E., Arnaboldi, M., Bournaud, F., Combes, F., Sparke, L. S., van Driel, W., & Capaccioli, M. 2003, ApJ, 585, 730
Jimenez, R., Verde, L., & Oh, S. P. 2003, MNRAS, 339, 243
Jing, Y. P., & Suto, Y. 2002, ApJ, 574, 538
Johnston, K. V., Law, D. R., & Majewski, S. R. 2005, ApJ, 619, 800
Kalapotharakos, C., Voglis, N., & Contopoulos, G. 2004, A&A, 428, 905
Katz, N. 1991, ApJ, 368, 325
Kazantzidis, S., Kravtsov, A. V., Zentner, A. R., Allgood, B., Nagai, D., & Moore, B. 2004, ApJ, 611, L73
Kazantzidis, S., Magorrian, J., & Moore, B. 2004, ApJ, 601, 37
Klypin, A., Gottlöber, S., Kravtsov, A. V., & Khokhlov, A. M. 1999, ApJ, 516, 530
Kochanek, C. S. 1995, ApJ, 445, 559
Koopmans, L. V. E., de Bruyn, A. G., & Jackson, N. 1998, MNRAS, 295, 534
Kuijken, K., & Tremaine, S. 1994, ApJ, 421, 178
Lake, G., & Norman, C. 1983, ApJ, 270, 51
Macciò, A. V., Sideris, I., Miranda, M., Moore, B., & Jesseit, R. 2007, ArXiv e-prints, 704
Mashchenko, S., Couchman, H. M. P., & Wadsley, J. 2006, Nature, 442, 539
Mayer, L., Kazantzidis, S., Mastropietro, C., & Wadsley, J. 2007, Nature, 445, 738
Merritt, D., & Fridman, T. 1996, ApJ, 460, 136
Merritt, D., & Quinlan, G. D. 1998, ApJ, 498, 625
Moore, B., Ghigna, S., Governato, F., Lake, G., Quinn, T., Stadel, J., & Tozzi, P. 1999, ApJ, 524, L19
Moore, B., Kazantzidis, S., Diemand, J., & Stadel, J. 2004, MNRAS, 354, 522
Norman, C. A., May, A., & van Albada, T. S. 1985, ApJ, 296, 20
Oguri, M., Lee, J., & Suto, Y. 2003, ApJ, 599, 7
Poon, M. Y., & Merritt, D. 2002, ApJ, 568, L89
Porciani, C., Dekel, A., & Hoffman, Y. 2002, MNRAS, 332, 325
Read, J. I., Goerdt, T., Moore, B., Pontzen, A. P., Stadel, J., & Lake, G. 2006, MNRAS, 373, 1451
Sackett, P. D., & Sparke, L. S. 1990, ApJ, 361, 408
Schoenmakers, R. H. M., Franx, M., & de Zeeuw, P. T. 1997, MNRAS, 292, 349
Schwarzschild, M. 1979, ApJ, 232, 236
Schweizer, F., Whitmore, B. C., & Rubin, V. C. 1983, AJ, 88, 909
Shen, J., & Sellwood, J. A. 2004, ApJ, 604, 614
Spergel, D. N., & et al. 2006, astro-ph/0603449
Stadel, J. G. 2001, Ph.D. Thesis, University of Washington
Statler, T. S. 1987, ApJ, 321, 113
Tonini, C., Lapi, A., & Salucci, P. 2006, ApJ, 649, 591
Udry, S., & Martinet, L. 1994, A&A, 281, 314
Valluri, M., & Merritt, D. 1998, ApJ, 506, 686
Warren, M. S., Quinn, P. J., Salmon, J. K., & Zurek, W. H. 1992, ApJ, 399, 405
Weinberg, M. D., & Katz, N. 2007, MNRAS, 375, 425
Zentner, A. R., Kravtsov, A. V., Gnedin, O. Y., & Klypin, A. A. 2005, ApJ, 629, 219